HHS Public Access

Author manuscript

Cell Rep. Author manuscript; available in PMC 2016 August 31.

Published in final edited form as:

Cell Rep. 2016 August 23; 16(8): 2077–2086. doi:10.1016/j.celrep.2016.07.046.

Structure of Gremlin-2 in complex with GDF5 gives insight into DAN-family mediated BMP antagonism

Kristof Nolan[1], **Chandramohan Kattamuri**[1], **Scott A. Rankin**[2], **Randy J. Read**[3], **Aaron M. Zorn**[2], and **Thomas B. Thompson**[1,*]

[1]Department of Molecular Genetics, Biochemistry, and Microbiology, the University of Cincinnati, Cincinnati, Ohio 45267 [2]Perinatal Institute, Cincinnati Children's Research Foundation and Department of Pediatrics, the University of Cincinnati, Cincinnati, Ohio 45229 [3]Department of Haematology, Cambridge Institute for Medical Research, University of Cambridge, Cambridge CB2 0XY, England.

Summary

The DAN-family, including Gremlin-1 and Gremlin-2 (Grem1 and Grem2), represents a large family of secreted BMP antagonists. However, how DAN proteins specifically inhibit BMP signaling has remained elusive. Here, we report the structure of Grem2 bound to GDF5 at 2.9 Å resolution. The structure reveals two Grem2 dimers binding perpendicularly to each GDF5 monomer, resembling an H-like structure. Comparison to the unbound Grem2 structure reveals a dynamic N-terminus that undergoes significant transition upon complex formation, leading to simultaneous interaction with the type I/type II receptor motifs on GDF5. Binding studies show that DAN-family members can interact with BMP-type I receptor complexes, whereas Noggin outcompetes the type I receptor for ligand binding. Interestingly, Grem2-GDF5 forms a stable aggregate-like structure, *in vitro,* not clearly observed for other antagonists, including Noggin and Follistatin. These findings exemplify the structural and functional diversity across the various BMP antagonist families.

Graphical abstract

*Correspondence: tom.thompson@uc.edu.

Author Contributions

KN, CK, and TBT designed and performed the experiments. KN and TBT wrote the manuscript. SAR and AMZ performed and designed the *in vivo* experiments. RJR provided necessary input for the crystallographic analysis of Grem2-GDF5.

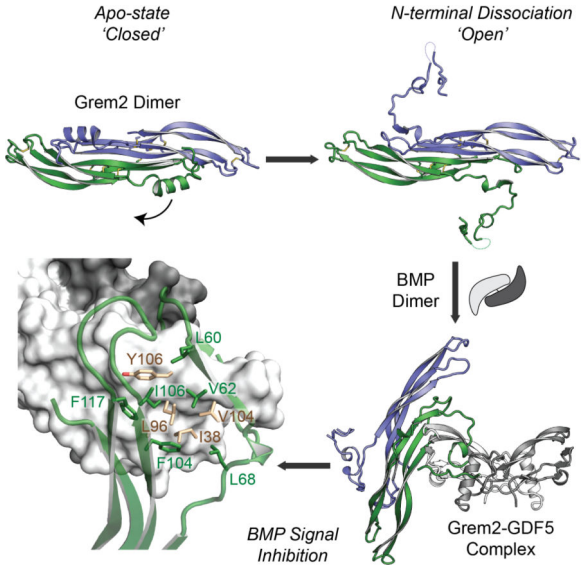

Introduction

The bone morphogenetic proteins (BMPs) and growth and differentiation factors (GDF) play many pivotal roles in biology, where their misregulation is central in numerous disease-state pathologies, including kidney and lung fibrosis, pulmonary arterial hypertension (PAH), and numerous cancers and skeletal diseases (Bragdon et al., 2011; Brazil et al., 2015). As such, regulation of BMP signaling is critical during both development and adult homeostasis.

Extracellular regulation of BMP signaling is dominated by the action of secreted protein antagonists that function to sequester BMP ligands and prevent receptor activation. While BMP ligands show significant structural conservation, their antagonist counterparts are strikingly diverse, ranging from small single domain proteins (e.g. Noggin and the DAN-family) to large multi-domain proteins (e.g. Chordin, Crossveinless-2 (CV2), Follistatin and GASP) (Brazil et al., 2015). Despite their importance, the structural basis of their activity is poorly understood as only two BMP-bound antagonist crystal structures have been solved. These include Noggin in complex with BMP7 and a binding domain of CV2 in complex with BMP2 (Groppe et al., 2002; Zhang et al., 2008). In both cases, these antagonists were shown to compete for both type I and type II receptor binding motifs on BMP, a common structural theme also identified for Follistatin-family antagonists (Mueller and Nickel, 2012; Thompson et al., 2005). However, these antagonist families exhibit vastly different binding mechanisms and structures, making it difficult to predict how uncharacterized antagonist families achieve inhibition.

The DAN-family includes Gremlin-1 (Grem1) and Gremlin-2 (Grem2 or PRDC), Coco, Cerberus, NBL1 (Dan), USAG-1 (Wise), and Sclerostin (SOST), most of which have been shown to directly inhibit BMP signaling (Nolan and Thompson, 2014). Furthermore, members of the DAN-family have been directly linked to various pathologies, including PAH, chronic kidney diseases (CKDs), and cancer, through their interactions with BMPs (Cahill et al., 2012; Dolan et al., 2005; Gao et al., 2012; Karagiannis et al., 2015; Yanagita et

al., 2006). In addition, Grem2, which is well conserved with Grem1 (68% identical), has been linked to atrial specific cardiomyocyte differentiation and hypertrophy (Müller et al., 2012; Tanwar et al., 2014). As such, structure/function studies of DAN-BMP interactions could help progress our ability to target these proteins in disease.

Here, we present the crystal structure of Grem2 bound to GDF5 at 2.9 Å resolution. Similar to other antagonists, Grem2 binds both the type I and type II receptor binding motifs on GDF5. However, unlike other known BMP-antagonist structures, two independent Grem2 dimers bind perpendicular to each GDF5 monomer, requiring only one monomer per Grem2 dimer to form this interaction and forming potential transient and stable complexes with the binary BMP-type I receptor complex.

Results

Structure of Grem2-GDF5

Previously, we solved the structure of Grem2 and began characterizing how it functionally inhibits BMP signaling (Nolan et al., 2013). To extend these studies, we sought to determine the structure of Grem2 in complex with BMP. As initial attempts using the high-affinity ligand BMP2 proved intractable, (see Supplementary Methods), we pursued alternative BMP ligands and readily determined the structure of Grem2 bound to its moderate affinity ligand, GDF5, to 2.9 Å resolution (Figure 1A and S1; Table S1). GDF5, while not often studied in light of the DAN-family, is able to bind Grem2 with appreciable affinity (K_D 146 nM) as compared to BMP2 (K_D 9 nM) when tested by surface plasmon resonance (SPR) (Figure S2A; Table S2). While the Grem2-BMP2 structure was desired, we hypothesized the Grem2-GDF5 structure would prove as useful and reveal the full extent of the DAN-BMP interaction.

Using a ligand centric view, two Grem2 dimers are found bound perpendicularly to the distal ends of the GDF5 dimer, generating internal C2 symmetry across the ligand (Figures 1A and 1B). Interestingly, each Grem2 monomer exclusively interacts with one GDF5 dimer, leaving the opposing Grem2 monomer open to interact with an additional GDF5 (Figure 1A). This 2:1 Grem2-GDF5 complex is generated by expanding the asymmetric unit (ASU), which contains two exclusive 1:1 dimer:dimer complexes of Grem2-GDF5 (Figure S1).

Previously, we showed that the structure of Grem2 (PDB: 4JPH) exhibits a growth factor-like fold, including a central cysteine-rich domain (CRD), or DAN-domain, which is flanked by N- and C-terminal extensions (Nolan et al., 2013). Using classical TGF-β ligand naming conventions, the DAN domain is divided into pairs of long anti-parallel β-strands, termed finger 1 (F1) and finger 2 (F2), with a wrist region (W) that connects the two fingers (Figure 1C). The structure of Grem2-GDF5 reveals that the core domain of Grem2 binds the convex surface of GDF5 using residues near or within the wrist of Grem2, while its N-terminus engages the apical surface of GDF5 and threads into the concave surface formed by GDF5 dimerization (Figure 1A). Similar to other known antagonists, Grem2 is found occupying interfaces on GDF5 consistent with both the type I (concave surface) and type II (convex surface and knuckle region) receptor-binding motifs (Figures 1A, 1D, and 3A) (Mueller and Nickel, 2012).

Comparing the unbound and GDF5 bound forms of Grem2 illustrates that a number of structural changes occur upon BMP binding, despite an RMSD of 2.0 Å across all Cα's. Most noticeably, the N-terminus of Grem2 undergoes drastic change upon ligand binding (RMSD of 8.5 Å for the N-terminus, 1.4 Å for the DAN-domain) (Figure 1C). In the apo state, Grem2 contains α-helices that lie over the DAN-domains of the dimer, partially blocking a significant portion of the BMP binding epitope (Figure 1C) (Nolan et al., 2013). Upon binding GDF5, these helices mostly disassociate from the DAN domain to wrap over the fingers of GDF5 and insert into the concave surface of the ligand (Figures 1A and 1C). Not only does this conformational change result in contacts between the N-terminus of Grem2 and GDF5, but also acts to expose underlying residues within the wrist and DAN domain of Grem2 that interact with the convex surface of the ligand. For GDF5, only slight structural changes are observed upon Grem2 binding (RMSD of 0.5 Å across all Cα's), consistent with the prescribed rigid and non-flexible nature of BMP subclass ligands (Figure 1D) (Mueller and Nickel, 2012).

Taking a detailed look at the interfaces between Grem2 and GDF5, 4 main regions can be described (Figures 2A-E): I) N-terminus of Grem2 binding the concave surface of GDF5 (960 $Å^2$), II) N-terminus of Grem2 hydrogen bonding the apical surface of GDF5 at the knuckle region of finger 2 (230 $Å^2$), III) wrist of Grem2 binding the convex surface of GDF5 (540 $Å^2$), and IV) C-terminus of Grem2 binding the finger 1 loop of GDF5 (310 $Å^2$); (total buried surface area of 1822 $Å^2$). For interface I, hydrophobic residues from the N-terminus of Grem2 interact with hydrophobic amino acids on both the proximal and distal GDF5 monomers. In addition, 3 hydrogen bonds are formed within this interface, specifically the backbone amide and carbonyl from A54 and the carbonyl of Y34 from Grem2 with the N64 side chain and L56 carbonyl of the distal GDF5 monomer (Figure 2B). Interestingly, mutation of this asparagine in GDF5 (N64K) has been linked to multiple synostosis syndrome (SYM1) and loss of Noggin based inhibition (Seemann et al., 2009). Additionally, the N-terminal interaction of Grem2 with GDF5 is likely stabilized by interface II, where backbone mediated hydrogen bonds form a small β-sheet between L60-R65 in Grem2 and N102-Y106 in GDF5 (Figure 2C).

For interface III, Grem2 again binds GDF5 utilizing extensive hydrophobic contacts. Here, residues within the wrist/DAN-domain (F104, I106, and F117) and N-terminus of Grem2 (L60, V61, and V62) interact with the convex hydrophobic surface of GDF5 finger 2, created by residues I38, L96, V104, and Y106 (Figure 2D). Lastly, the C-terminus of Grem2 interacts with the helical turn within finger 1 of GDF5 (interface IV) through hydrophobic, polar, and ionic interactions (Figure 2E). Combined, interface III and IV compose a large binding interface between Grem2 and GDF5 (845 $Å^2$), likely contributing a large majority of the Grem2-BMP interaction.

Mutational Analysis of the Grem2 BMP-binding Epitope

Using the Grem2-GDF5 structure as a model, we wanted to determine if the Grem2 interface was consistent between the low affinity ligand, GDF5, and the better studied, high affinity target of the DAN-family, BMP2. We previously identified several amino acids in Grem2 and NBL1 important for BMP2 mediated inhibition and directly correlated decreases in

binding affinity with decreases in cell- and *in vivo*-based signaling (Figure 2F) (Nolan et al., 2013; 2015). Furthermore, these previously identified amino acids are central to interface III.

While these studies provided insight into the location of the BMP binding epitope, even the most disrupting mutations in Grem2 maintained significant activity (Nolan et al., 2013). This is consistent with the extensive interaction revealed in the Grem2-GDF5 structure. Therefore, we extended our mutational analysis to more effectively disrupt these hydrophobic interfaces by modulating a series of Grem2 residues. As such, we generated the I106A, I106A/F117A, F104A/F117A, and F104A/I106A/F117A mutants (interface III) and the I49D/V52D/L53D mutant (interface I) (Figures 2B and 2D). Previously, we identified F104 and F117 as significant contributors to the BMP interaction, where mutation of these to alanine gave a 49-fold (3.5-fold in NBL1) and 63-fold increase in the IC_{50} (or decrease in activity) of Grem2 for BMP2, respectively, as well as corresponding decreases in binding K_D's as determined by SPR (Nolan et al., 2015; 2013).

Grem2 mutants were tested for their ability to inhibit both BMP2 and GDF5 based signaling in osteoblast cells stably transfected with a BMP-responsive promoter (Yadav et al., 2012). As expected, these mutants significantly decreased the ability of Grem2 to inhibit both BMP2 and GDF5 signaling, where this effect increased with the number of mutations introduced into interface III. For F104A/I106A/F117A, nearly all inhibition was lost towards both BMP2 and GDF5 (721-fold and 8-fold increase in IC_{50}, respectively) (Figures 2E and S2B; Table S3). For I49D/V52D/L53D, only minor comparative increases were seen in IC_{50} values for BMP2 and GDF5 (2.9-fold and 1.2-fold, respectively), suggesting that interface I and the N-terminus of Grem2 only modestly contribute to overall BMP-based inhibition (Figures 2E and S2B; Table S3). Furthermore, these findings are consistent with amino acid conservation across the DAN-family, as F104, I106, and F117 are mostly conserved across the stronger BMP-antagonizing members (Grem1, Coco, NBL1) and poorly in SOST and USAG-1, while I49, V52, and L53 show no significant conservation (Figure S2C).

Next, we tested our Grem2 mutants in developing *Xenopus* embryos, which require functional BMP4 and BMP7 signaling for proper development. Microinjection of BMP antagonists, such as Grem2, into the developing embryo can inhibit endogenous BMP ligands, resulting in loss of ventral-posterior structures (e.g. the tail) and loss of direct BMP-target gene expression (e.g. *sizzled*). Our results show that Grem2 mutants at interface III maintain no ability to inhibit downstream *sizzled* expression and tail growth and elongation as compared to wild-type, resembling BSA control experiments (Figures 2G and 2H). This finding correlates well with our luciferase reporter results for both BMP2 and GDF5 based signaling, suggesting a generality for Grem2-based BMP inhibition *in vitro* and *in vivo*.

Receptor Based Mechanism of Grem2 mediated BMP Inhibition

A growing theme with extracellular BMP antagonists is their ability to block ligand-receptor interactions, where antagonists directly interact with surfaces associated with type I/type II receptor binding (Figures 3A and 3B) (Mueller and Nickel, 2012). To better illustrate this, we colored the surfaces of the ligand structures and aligned sequences that interact with Grem2, Noggin, Follistatin, CV2, and the type I/type II receptors (Figure S3AS3C). This analysis clearly shows that each antagonist utilizes highly conserved areas consistent with

the receptor binding motifs on BMP. However, comparison of Grem2 and Noggin depicts very different BMP-binding strategies. Noggin, a disulfide-bonded dimer, binds on the apical side of the ligand, simultaneously interacting with all 4 receptor sites, whereas two Grem2 molecules, similar to CV2, independently block each end of the ligand (Figures 3A and 3B). Therefore, we sought to determine if Grem2 functionally blocks type I and type II receptor binding to BMP similar to Noggin (Groppe et al., 2002; Zimmerman et al., 1996).

For these experiments, we mixed various ratios of Grem2 and Noggin with BMP2 (molar ratio of 0.1:1 to 2:1 antagonist to BMP) and tested their ability to bind to immobilized Alk3-Fc and BMPR2-Fc receptors using SPR. As shown, Grem2 blocks binding of BMP2 to BMPR2 at ratios near or greater than 1:1, as expected based upon the extensive Grem2-GDF5 interface III, similar to Noggin (Figures 3C and S3D). In addition, Grem2 blocked BMP2 binding to Alk3 at a ratio of 2:1, consistent with the stoichiometry of the Grem2-GDF5 complex (Figure 3D). In contrast, Noggin only requires a 1:1 ratio to completely block BMP2 binding to Alk3, consistent with the structure of Noggin-BMP7 (Figure S3E).

To generalize our findings for Grem2 to the rest of the DAN-family, we extended our analysis to the moderate BMP antagonist, NBL1. Expectedly, NBL1 blocked BMP2 binding to BMPR2 similar to Grem2 (Figure 3F). Interestingly, NBL1 did not block BMP2 binding to Alk3 even at a 2:1 ratio (Figure 3G). Furthermore, at certain ratios, and 0.5:1 to 2:1 for NBL1:BMP2 and even 0.5:1 for Grem2:BMP2, the total response increased as compared to the BMP2 control, possibly indicating binding of DAN-BMP complexes to Alk3 (Figures 3D and 3G). With this in mind, we wanted to test more directly whether or not Grem2 and NBL1 lacked the ability to block type I receptor binding or whether potential ternary DAN-BMP-type I receptor complexes were forming.

To test DAN-BMP-type I receptor complex formation, SPR was performed using immobilized Alk3-Fc. For each experiment, BMP2 was injected to form the binary BMP2-Alk3 complex on the chip, followed by direct injection of Grem2, NBL1, or Noggin. Unexpectedly, both Grem2 and NBL1 showed a significant ability to bind the BMP2-Alk3 complex. While Grem2 showed a relatively fast dissociation rate, NBL1 formed a stable ternary complex with BMP2-Alk3 (Figures 3E and 3H). This difference is likely explained by the short N-terminus of NBL1, which lacks the length necessary to traverse into the type I receptor-binding motif of BMPs (Nolan and Thompson, 2014). Interestingly, the binding of Grem2 and NBL1 never drops below the response level of ligand binding alone, suggesting that a transient (Grem2) or stable (NBL1) inhibitory DAN-BMP-type I receptor complex can form (Figures 3E and 3H). In contrast, Noggin binding to the BMP2-Alk3 complex dissociates very rapidly, where the generated response drops well below the levels for BMP2 binding alone, suggesting Noggin strips BMP2 away from Alk3 (Figure 3I). In addition, each antagonist (Grem2, NBL1, and Noggin) showed no ability to form a potential ternary complex with BMP2 and BMPR2, likely due to the rapid dissociation of the BMP2-BMPR2 complex (Figure S3F).

Next, we wanted to determine if the SPR response following Noggin treatment (as mentioned above) could be restored to that of the BMP2 alone binding to Alk3. This injection caused the response curves to closely match those of the initial BMP2 injection,

suggesting Noggin removed the majority of BMP2 from Alk3 (Figure 3J). For Grem2 and NBL1, injection of additional BMP2 resulted in a higher maximal response when compared to BMP2 alone (Figure 3J). This heightened response is dependent upon prior injection of Grem2 or NBL1 and suggests formation of a DAN-BMP-type I receptor complex.

Lastly, we recapitulated our SPR findings using an ELISA-based assay. For these experiments, Alk3-Fc was immobilized. Fluorescently labeled BMP2 was then added to wells containing Alk3-Fc, incubated, and excess ligand was washed away. Wells were then treated with either Grem2 or Noggin and fluorescence was measured in the supernatant to determine if BMP2 was dissociating from Alk3-Fc. As expected, Grem2 did not significantly increase the amount of BMP2 in the supernatant (Figure 3K). However, Noggin drastically increased the levels of BMP2 in the supernatant, supporting that Noggin can remove BMP2 from Alk3 (Figure 3K).

Grem2-BMP Ordered Aggregate Formation

In the Grem2-GDF5 structure, one monomer of Grem2 interacts with one dimer of GDF5, leaving the opposing Grem2 monomer open to bind another GDF5 ligand. Upon generating symmetry outside of the ASU, a larger, alternating and ordered aggregate-like structure is formed between Grem2 and GDF5, where each monomer propagates to a new interaction partner, seemingly *ad infinitum*, and possibly explaining the extreme insolubility of purified Grem2-BMP complexes (Figure 4A; see Supplemental Methods).

To test whether this alternating aggregate could be produced *in vitro*, we utilized SPR. First, we injected Grem2 over a BMP2 amine coupled chip to form the Grem2-BMP complex, followed by additional alternation injections of Grem2 and BMP2. Agreeing with our structure, these alternating injections resulted in a continuously additive binding response, illustrating the ordered aggregate-like nature of this interaction (Figure 4B). Furthermore, this response is dependent upon alternation of Grem2 and BMP2, where Grem2 followed by Grem2 or BMP2 followed by BMP2 could not recapitulate this effect (Figure S4). NBL1 also exhibits this ordered aggregate-like formation when tested with BMP2, albeit less efficiently (Figure 4B). Additionally, recent evidence suggests a similar mechanism for Grem1 and BMP2 using assays synonymous to SPR (Kisonaite et al., 2016).

We next performed a similar analysis with Follistatin and Noggin. Not surprisingly, Follistatin did not exhibit any ordered aggregation with Activin A (Figure 4E). For Noggin, however, this effect was observed to some degree (Figure 4C). Despite this, the off-rate of Noggin in this state was much faster as compared to Noggin alone with BMP2. Taking into account that Noggin exists as a functional dimer, it is not surprising to find some, albeit likely unfavorable, ability to form these larger-order complexes (Groppe et al., 2002). To directly compare Noggin and Grem2, we performed injections at a slower flow rate with longer association/dissociation times for 3 consecutive alternating injections of ligand and antagonist. Although both proteins form higher-order aggregates, the maximal response for each alternating Grem2 and BMP2 injection remains highly sustained while those for Noggin and BMP2 showing a decreasing trend with each subsequent injection (Figure 4D). This suggests chain-growing as a non-ideal, thermodynamically unfavorable mechanism for Noggin inhibition but very likely for Grem2 in the *in vitro* context (Figure 4D).

Discussion

In this study, we present the structure of Grem2 bound to GDF5. Through analysis of this structure, numerous features have been revealed, distinguishing the DAN-family of BMP-antagonists from other ligand-antagonist structures (e.g. CV2-BMP2, Noggin-BMP7, Follistatin-Activin A) (Groppe et al., 2002; Thompson et al., 2005; Zhang et al., 2008). Furthermore, the Grem2-GDF5 structure supports the theme that structurally diverse families of antagonists have evolved to recognize structurally conserved BMP ligands.

Analysis of the Grem2-GDF5 structure reveals a number of features consistent with our previous findings, such as the importance of F104 and F117 in Grem2-based BMP antagonism, where we directly correlated decreases in binding to losses in cell-based and *in vivo* signal inhibition (Nolan et al., 2013). Furthermore, this structure has revealed the full extent of the BMP-binding interface, where 4 main interfaces can be described (Figure 2). In our analysis, we found that mutation of F104, I106, and F117, central to interface III, significantly reduced the ability of Grem2 to inhibit both BMP2 and GDF5 signaling (Table S3). Unexpectedly, the Grem2-GDF5 structure shows that Grem2 utilizes both its N- and C-termini to bind GDF5 and stabilize the complex through both hydrophobic and polar interactions.

Like other known BMP binding partners, the N-terminus of Grem2 forms numerous intimate contacts with the concave surface of GDF5. As such, a pivotal ‘knob-in-hole’ feature has been described for BMP binding to Alk3 (F85), Noggin (P35), and CV2 (I2) (Groppe et al., 2002; Keller et al., 2004; Zhang et al., 2008). Similarly for Grem2, L53 is positioned within this same hydrophobic cleft on GDF5 (Figure 2B). However, this residue, amongst others in interface I, does not appear to play a significant role in BMP signal antagonism as the I49D/V52D/L53D mutant exhibited near wild-type activity (Table S3).

Similar to other antagonists, Grem2 engages BMP through using its receptor binding motifs (Figure 3 and S3). Furthermore, CV2, Noggin, and Grem2 all utilize N-terminal extensions to traverse the apical surface of the ligand to extend into the type I receptor-binding motif (Groppe et al., 2002; Zhang et al., 2008). However, SPR analysis shows that, unlike Noggin, Grem2 possibly forms a transient DAN-BMP-type I complex, similar to that seen for Follistatin and BMP4 (Figure 3E and 3I) (Iemura et al., 1998). NBL1 shares this characteristic with Grem2, although the dissociation is much slower, indicating a more stable ternary complex (Figure 3E and 3H). This is possibly due to the short N-terminus in NBL1, which likely cannot traverse into the concave epitope of BMP (Nolan and Thompson, 2014). In addition, Cerberus has recently been shown bock Nodal binding to its type II receptor, similar to Grem2 and NBL1. Differently, Cerberus also blocks ligand-type I receptor binding, where processing of its extraordinarily long N-terminus may function to modulate its ability to inhibit specific ligand-receptor binding events (Aykul and Martinez-Hackert, 2016). As such, future studies should aim at determining the role of the variable DAN-family N-terminus in inhibition of ligand-receptor interactions, if DANBMP-type I receptor complexes exist in the physiological context, and what impact these complexes exert on BMP signaling, such as a dominant-negative effect on signaling.

Based upon the similarity of the apo-Grem2 dimer structure to that of NBL1 and the recently solved structure of Grem1, we hypothesize that conserved epitopes are utilized across the DAN-family to inhibit BMPs (Kisonaite et al., 2016; Nolan et al., 2015; 2013). Physiologically, Grem1 is the most well studied of all DAN-family antagonist and has been shown to be critical in numerous aspects of mammalian biology and disease (Brazil et al., 2015). To extend our structural analysis to Grem1, we generated models of the Grem1-BMP2 and Grem2-BMP2 complexes. These models strongly correlate with our current findings, showing that the type II interface of BMP2 is central to the interaction and nearly identical with that seen for Grem2-GDF5 (Figure S3DS3K). As expected, F104, I106, and F117 (F125, I127, and F138 in Grem1) are central in this predicted interface, suggesting a conserved mechanism for Grem1 and Grem2 mediated inhibition of both GDF5 and BMP2. Consistent with this, it was recently shown that specific amino acids at the BMP2 type II interface are important for Grem1 binding (Kisonaite et al., 2016).

Further diversifying the Grem2-GDF5 structure from those of Noggin, CV2, and Follistatin, is the ability of this complex to propagate and form ordered aggregate-like structures *in vitro*, a notion supported though our structural and SPR analyses (Figure 4). As one monomer of Grem2 directly interacts with one pair of type I/II motifs on the GDF5 dimer, this leaves the adjacent Grem2 monomer open to bind an additional GDF5 ligand (Figure 4A). Our data also indicates that NBL1 exhibits this phenotype, albeit to a lesser degree (Figure 4B). Recent studies also suggest that Grem1 can form oligomeric complexes when binding to BMP2 (Kisonaite et al., 2016). It will be interesting to determine if this mechanism is generally consistent across the DAN-family. Furthermore, future studies should aim to verify the existence of these alternating higher-order aggregates *in vivo*, perhaps through the use of super resolution confocal microscopy. In addition, if DAN-family heterodimers can be generated (e.g. wild-type/binding-deficient mutant), this would allow for the exploration of the necessity and mechanistic role of these aggregation events in BMP signal inhibition.

In conclusion, the structure of Grem2-GDF5 has revealed a number of key findings for DAN-family mediated BMP inhibition. These findings increase our general understanding of DAN-family mediated BMP inhibition and reveal how structurally divergent antagonists have evolved unique mechanisms to inhibit BMP ligands.

Experimental Procedures

Protein expression and purification

Purified Grem2, GDF5, BMP2, NBL1, and Follistatin were generated utilizing previously published protocols (Cash et al., 2009; Einem et al., 2010; Nolan et al., 2015; 2013). Grem2 mutants were generated using the quickchange mutagenesis and produced similar to wild-type Grem2. All other protein components utilized for SPR or other experiments were purchased from RnD.

X-ray structure determination and refinement of Grem2-GDF5

Grem2 and GDF5 were mixed in 10 mM HCl and concentrated to 10 mg/ml in a 2:1 molar ratio. Grem2-GDF5 crystals were grown by hanging drop vapor diffusion using 100 mM HEPES pH 7.5, 1.4 M NH_4Cl, 4% ethylammonium nitrate, 20°C. Diffraction data were collected at the Advanced Photon Source (23-ID-D), Argonne National Laboratory. Initial phases were generated by molecular replacement using Phaser with the structures of Grem2 (4JPH) and GDF5 (1WAQ). Refinement was performed using Phenix with NCS. See Supplemental Experimental Procedures for details. Coordinates have been deposited in the Protein Data Bank (accession code 5HK5)

Surface plasmon resonance

All experiments were performed similarly to as previously described (Nolan et al., 2013). Briefly, BMP2, BMP4 (RnD), BMP7 (RnD), GDF5, Alk3-Fc (RnD), BMPR2-Fc (RnD), and Activin A (RnD) were immobilized to the surface of a CM5 sensor chip. For receptor binding experiments, protein A was immobilized followed by capture of Alk3-Fc or BMPR2-Fc or receptors were directly coupled. See Supplemental Experimental Procedures for details.

Luciferase reporter assays

A BMP responsive luciferase reporter osteoblast cell line, kindly provided by Dr. Amitabha Bandyopadhyay, was used to measure BMP activity as previously reported (Nolan et al., 2015). Cells were grown overnight in a 96-well plate and treated with DMEM/Hi Glucose for 4 h then treated with proteins for 3 h and monitored for luminescence. IC_{50} values were calculated using Prism Graphpad.

Xenopus embryo assay

Embryo manipulations and microinjections were performed as previously described and staged according to the normal table of development for *Xenopus laevis* (Nolan et al., 2013). See Supplemental Experimental Procedures for details.

ELISA Competition Assay

Alk3-Fc was immobilized to a 96-well ELISA plate at a concentration of 5 μg/ml. BMP2 was labeled using carboxyrhodamine (Molecular Dimensions, BMP2*). BMP2* was incubated with immobilized Alk3-Fc for 1 h at 1.5 μg/ml, washed with PBS, then incubated for 1 h with either Noggin or Grem2. Supernatant was then removed from each well and analyzed for fluorescence (BioTek Synergy H1). Controls included PBS alone, BMP2* alone, and BMP2* incubated with Alk3 for comparison.

Statistical Methods

Statistical significance was determined using the Student's *t*-test. All grouped data is represented as the mean ± standard error of the mean (SEM). All data for each experiment was performed, at a minimum, in triplicate to ensure reproducibility.

Supplementary Material

Refer to Web version on PubMed Central for supplementary material.

Acknowledgements

This work was supported by NIGMS (R01 GM114640) to TBT, the NIDDK (R01 DK070858) to AMZ, a PRF from the Wellcome Trust (Grant No. 082961/Z/07/Z) to RJR, and an AHA Fellowship (grant 14PRE20480142) to KN.

References

Aykul S, Martinez-Hackert E. New ligand binding function of human Cerberus and role of proteolytic processing in regulating ligand-receptor interactions and antagonist activity. J. Mol. Biol. 2016; 428:590–602. [PubMed: 26802359]

Bragdon B, Moseychuk O, Saldanha S, King D, Julian J, Nohe A. Bone morphogenetic proteins: a critical review. Cell. Signal. 2011; 23:609–620. [PubMed: 20959140]

Brazil DP, Church RH, Surae S, Godson C, Martin F. BMP signalling: agony and antagony in the family. Trends Cell Biol. 2015; 25:249–264. [PubMed: 25592806]

Cahill E, Costello CM, Rowan SC, Harkin S, Howell K, Leonard MO, Southwood M, Cummins EP, Fitzpatrick SF, Taylor CT, Morrell NW, Martin F, McLoughlin P. Gremlin plays a key role in the pathogenesis of pulmonary hypertension. Circulation. 2012; 125:920–930. [PubMed: 22247494]

Cash JN, Rejon CA, McPherron AC, Bernard DJ, Thompson TB. The structure of myostatin:follistatin 288: insights into receptor utilization and heparin binding. EMBO J. 2009; 28:2662–2676. [PubMed: 19644449]

Dolan V, Murphy M, Sadlier D, Lappin D, Doran P, Godson C, Martin F, O'Meara Y, Schmid H, Henger A. Expression of gremlin, a bone morphogenetic protein antagonist, in human diabetic nephropathy. Am. J. Kidney Dis. 2005; 45:1034–1039. [PubMed: 15957132]

von Einem S, Schwarz E, Rudolph R. A novel TWO-STEP renaturation procedure for efficient production of recombinant BMP-2. Protein Expr. Purif. 2010; 73:65–69. [PubMed: 20302941]

Gao H, Chakraborty G, Lee-Lim AP, Mo Q, Decker M, Vonica A, Shen R, Brogi E, Brivanlou AH, Giancotti FG. The BMP inhibitor Coco reactivates breast cancer cells at lung metastatic sites. Cell. 2012; 150:764–779. [PubMed: 22901808]

Groppe J, Greenwald J, Wiater E, Rodriguez-Leon J, Economides AN, Kwiatkowski W, Affolter M, Vale WW, Belmonte JCI, Choe S. Structural basis of BMP signalling inhibition by the cystine knot protein Noggin. Nature. 2002; 420:636–642. [PubMed: 12478285]

Iemura S, Yamamoto TS, Takagi C, Uchiyama H, Natsume T, Shimasaki S, Sugino H, Ueno N. Direct binding of follistatin to a complex of bone-morphogenetic protein and its receptor inhibits ventral and epidermal cell fates in early Xenopus embryo. Proc. Natl. Acad. Sci. U.S.A. 1998; 95:9337–9342. [PubMed: 9689081]

Karagiannis GS, Musrap N, Saraon P, Treacy A, Schaeffer DF, Kirsch R, Riddell RH, Diamandis EP. Bone morphogenetic protein antagonist gremlin-1 regulates colon cancer progression. Biol. Chem. 2015; 396:163–183. [PubMed: 25153376]

Keller S, Nickel J, Zhang JL, Sebald W, Mueller TD. Molecular recognition of BMP-2 and BMP receptor IA. Nat. Struct. Mol. Biol. 2004; 11:481–488. [PubMed: 15064755]

Kisonaite M, Wang X, Hyvönen M. Structure of Gremlin-1 and analysis of its interaction with BMP-2. Biochem. J. 2016; 473:1593–1604. [PubMed: 27036124]

Mueller TD, Nickel J. Promiscuity and specificity in BMP receptor activation. FEBS Lett. 2012; 586:1846–1859. [PubMed: 22710174]

Müller II, Melville DB, Tanwar V, Rybski WM, Mukherjee A, Shoemaker BM, Wang W-D, Schoenhard JA, Roden DM, Darbar D, Knapik EW, Hatzopoulos AK. Functional modeling in zebrafish demonstrates that the atrial-fibrillation-associated gene GREM2 regulates cardiac laterality, cardiomyocyte differentiation and atrial rhythm. Dis. Model Mech. 2012; 6:332–341. [PubMed: 23223679]

Nolan K, Kattamuri C, Luedeke DM, Angerman EB, Rankin SA, Stevens ML, Zorn AM, Thompson TB. Structure of Neuroblastoma Suppressor of Tumorigenicity 1 (NBL1): Insights for the Functional Variability Across Bone Morphogenetic Protein (BMP) Antagonists. J. Biol. Chem. 2015; 290:4759–4771. [PubMed: 25561725]

Nolan K, Kattamuri C, Luedeke DM, Deng X, Jagpal A, Zhang F, Linhardt RJ, Kenny AP, Zorn AM, Thompson TB. Structure of Protein Related to Dan and Cerberus: Insights into the Mechanism of Bone Morphogenetic Protein Antagonism. Structure. 2013; 21:1417–1429. [PubMed: 23850456]

Nolan K, Thompson TB. The DAN family: Modulators of TGF-β signaling and beyond. Protein Sci. 2014; 23:999–1012. [PubMed: 24810382]

Seemann P, Brehm A, König J, Reißner C, Stricker S, Kuss P, Haupt J, Renninger S, Nickel J, Sebald W, Groppe JC, Plöger F, Pohl J, Schmidt-von Kegler M, Walther M, Gassner I, Rusu C, Janecke AR, Dathe K, Mundlos S. Mutations in GDF5 reveal a key residue mediating BMP inhibition by NOGGIN. PLoS Genet. 2009; 5:e1000747. [PubMed: 19956691]

Tanwar V, Bylund JB, Hu J, Yan J, Walthall JM, Mukherjee A, Heaton WH, Wang W-D, Potet F, Rai M, Kupershmidt S, Knapik EW, Hatzopoulos AK. Gremlin 2 promotes differentiation of embryonic stem cells to atrial fate by activation of the JNK signaling pathway. Stem Cells. 2014; 32:1774–1788. [PubMed: 24648383]

Thompson TB, Lerch TF, Cook RW, Woodruff TK. The structure of the follistatin: activin complex reveals antagonism of both type I and type II receptor binding. Dev. Cell. 2005; 9:535–543. [PubMed: 16198295]

Yadav PS, Prashar P, Bandyopadhyay A. BRITER: a BMP responsive osteoblast reporter cell line. PLoS ONE. 2012; 7:e37134. [PubMed: 22611465]

Yanagita M, Okuda T, Endo S, Tanaka M, Takahashi K, Sugiyama F, Kunita S, Takahashi S, Fukatsu A, Yanagisawa M, Kita T, Sakurai T. Uterine sensitization-associated gene-1 (USAG-1), a novel BMP antagonist expressed in the kidney, accelerates tubular injury. J. Clin. Invest. 2006; 116:70–79. [PubMed: 16341262]

Zhang JL, Qiu LY, Kotzsch A, Weidauer S, Patterson L, Hammerschmidt M, Sebald W, Mueller TD. Crystal Structure Analysis Reveals How the Chordin Family Member Crossveinless 2 Blocks BMP-2 Receptor Binding. J. Mol. Biol. 2008; 14:739–750.

Zimmerman LB, De Jesús-Escobar JM, Harland RM. The Spemann organizer signal noggin binds and inactivates bone morphogenetic protein 4. Cell. 1996; 86:599–606. [PubMed: 8752214]

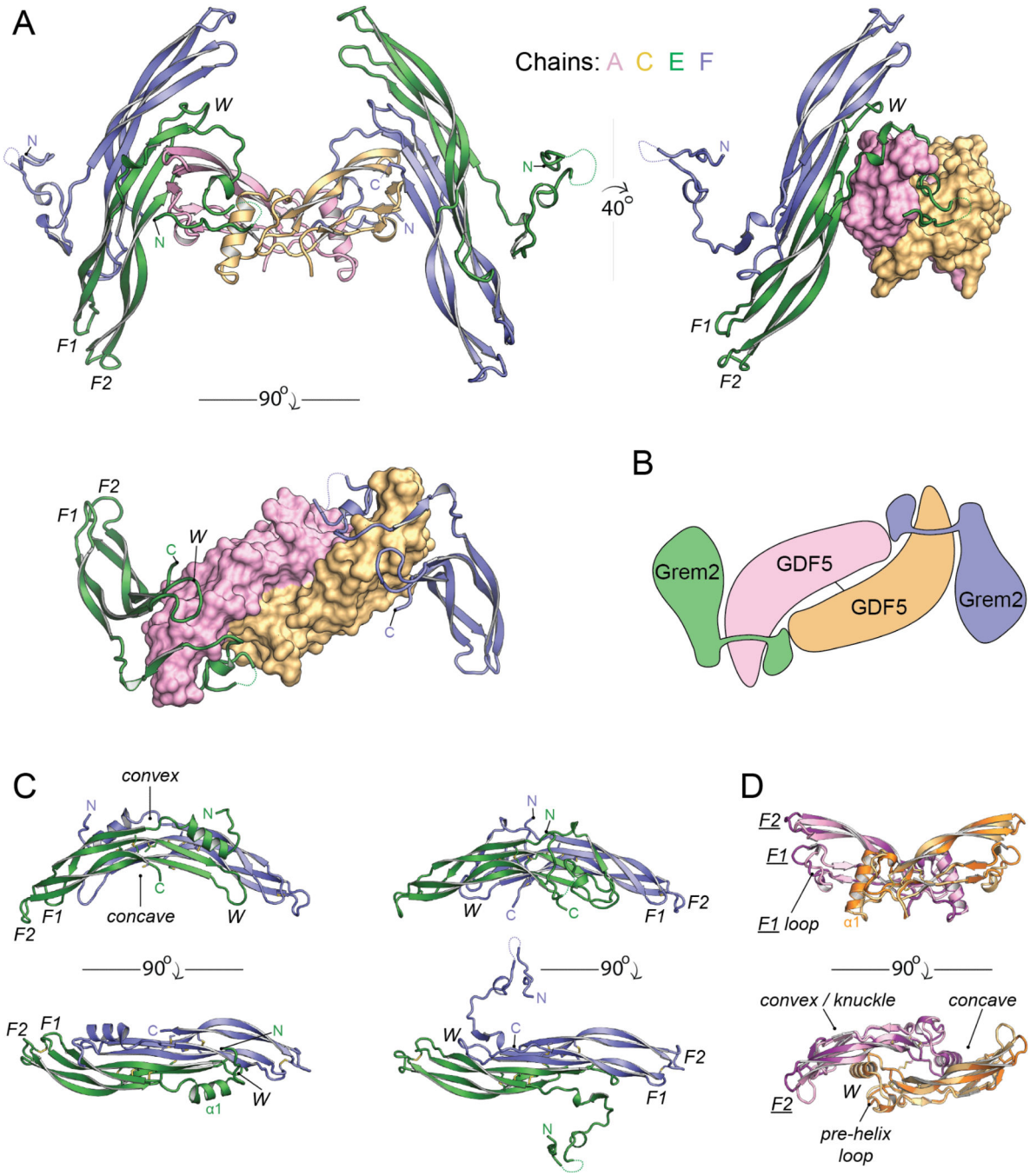

Figure 1. Structure of Grem2-GDF5

(A) Ribbon and surface representations of Grem2-GDF5 in a ligandcentric view. Grem2 (green, Chain E; blue, Chain F); GDF5 (pink, Chain A; gold, Chain C). (B) Schematic of the Grem2-GDF5 complex. (C) Grem2 in the apo state (left; PDB:4JPH) or GDF5 bound state (right). (D) Superposition of unbound GDF5 (dark purple/orange, PDB:1WAQ) and Grem2 bound (pink/gold). For Grem2 and GDF5 (underscored), F1, F2 and W correspond to finger 1, finger 2, and the wrist region. Dotted lines show unresolved amino acids 35-44 in Grem2.

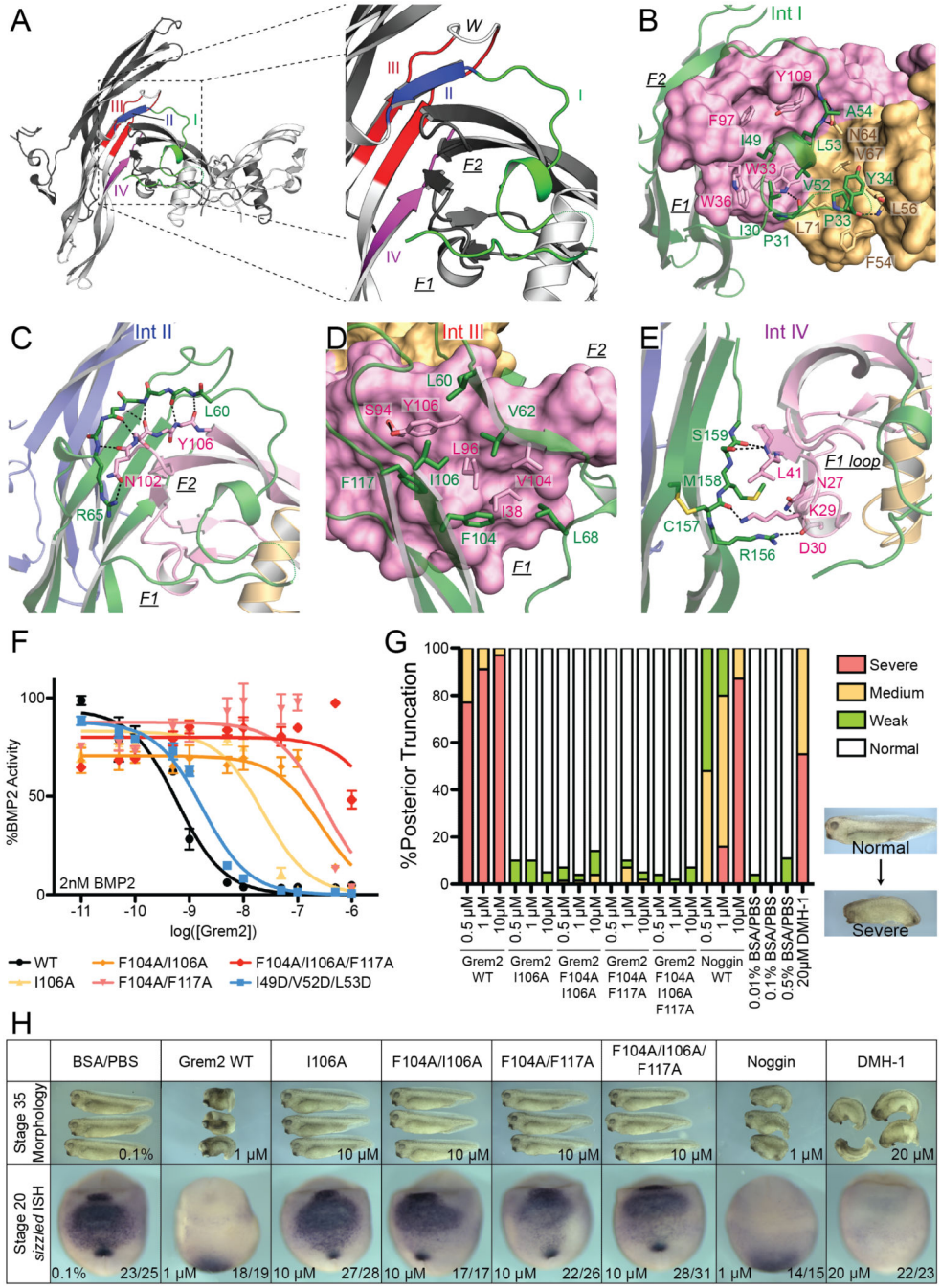

Figure 2. Grem2-BMP Binding Interface and Analysis

(A) Grem2-GDF5 complex with BMP-binding interfaces in Grem2 (labeled I through IV) highlighted in green, blue, red, and magenta, respectively. (B-E) Grem2 and GDF5 are colored as in Figure 1. Zoomed in view of the Grem2-GDF5 (B) interface I, (C) interface II, (D) interface III, and (E) interface IV as described in the text. (F) BMP-responsive luciferase reporter assay using a BMP-responsive osteoblast cell-line and showing titration of various Grem2 mutants against 2nM BMP2. Experiments were performed in triplicate. (G-H) Injection (stage 9) of wild type and Grem2 mutants (0.5 µM, 1 µM, and 10 µM) in

developing *Xenopus* embryos. Quantification (G) and representative images (H, top) of BMP-dependent axial development (stage 35). (H, bottom) *In situ* hybridization (stage 20) for mRNA expression of the BMP-target gene *sizzled*. Numbers in boxes indicate concentration of the reagent used (top and bottom) as well as the number of embryos scored (bottom).

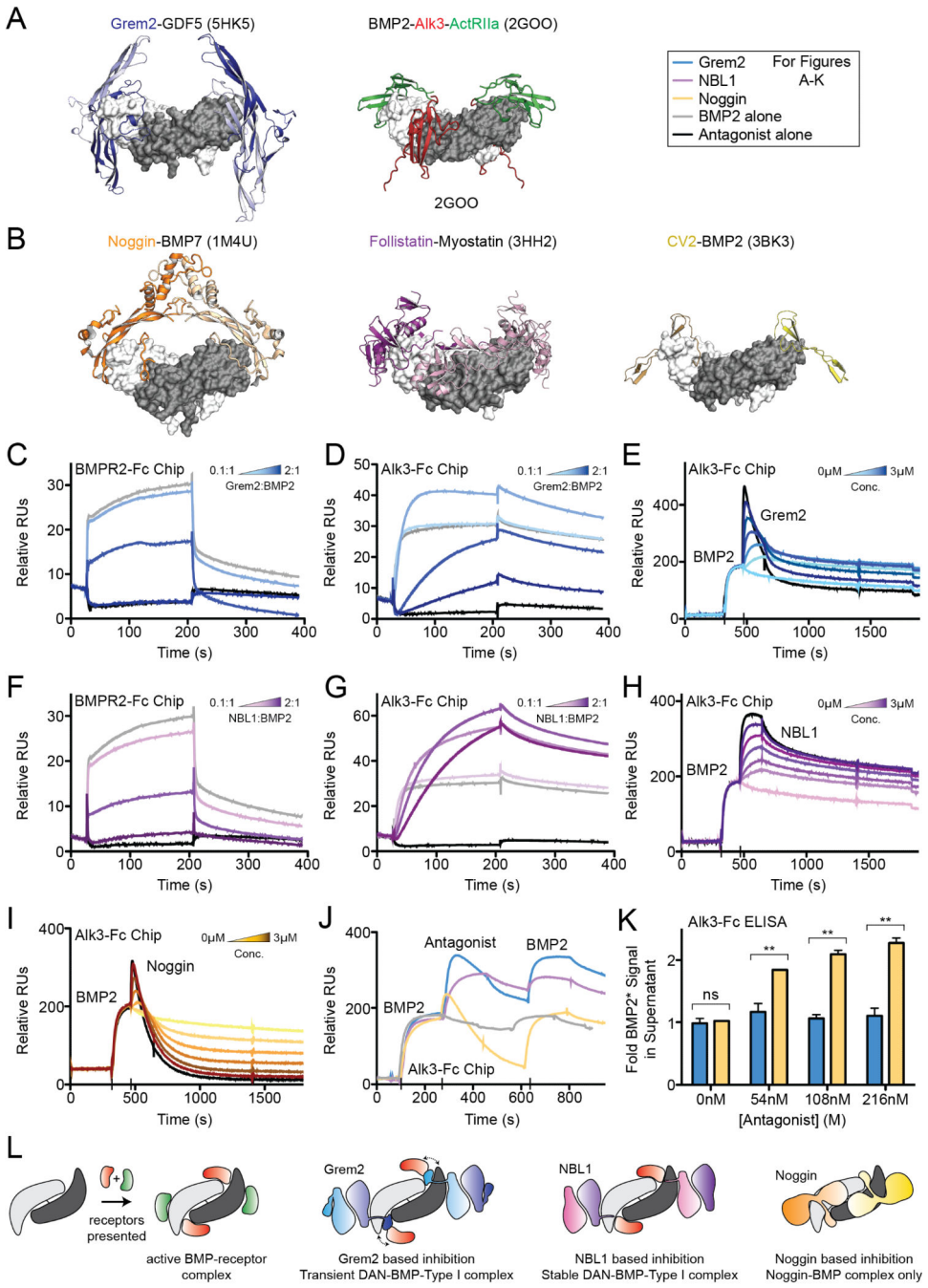

Figure 3. Differences in Antagonist Inhibition of Ligand-Receptor Interactions

(A-B) Structures of BMP-antagonist and BMP-receptor complexes. (C, D, F, G) SPR experiments injecting mixtures of (C-D) Grem2-BMP2 and (F-G) NBL1-BMP2 onto Alk3-Fc or BMPR2-Fc captured using a protein A chip. Molar ratios 0.1:1, 0.5:1, 1:1, and 2:1 of antagonist:ligand were tested. BMP2 was maintained at a constant 250 nM. (E, H, I) SPR experiments using immobilized Alk3. BMP2 (500 nM) was first injected to form the Alk3-BMP2 complex. Grem2 (E), NBL1 (H), or Noggin (I) were subsequently titrated (0-3 μM) and co-injected following BMP2. (J) SPR performed as in E, H, and I with an additional

BMP2 injection to determine if ligand binding could be recovered. (K) ELISA binding assay using immobilized Alk3-Fc treated with labeled BMP2, washed, and then treated with Grem2 (blue) or Noggin (orange) at various concentrations for 1 h. Fluorescence was measured in the supernatant to quantify BMP2 release from Alk3. ** = p-value < 0.05 using student's t-test. All experiments were performed in triplicate. (L) Schematic showing potential DAN-BMP-type I receptor ternary complexes.

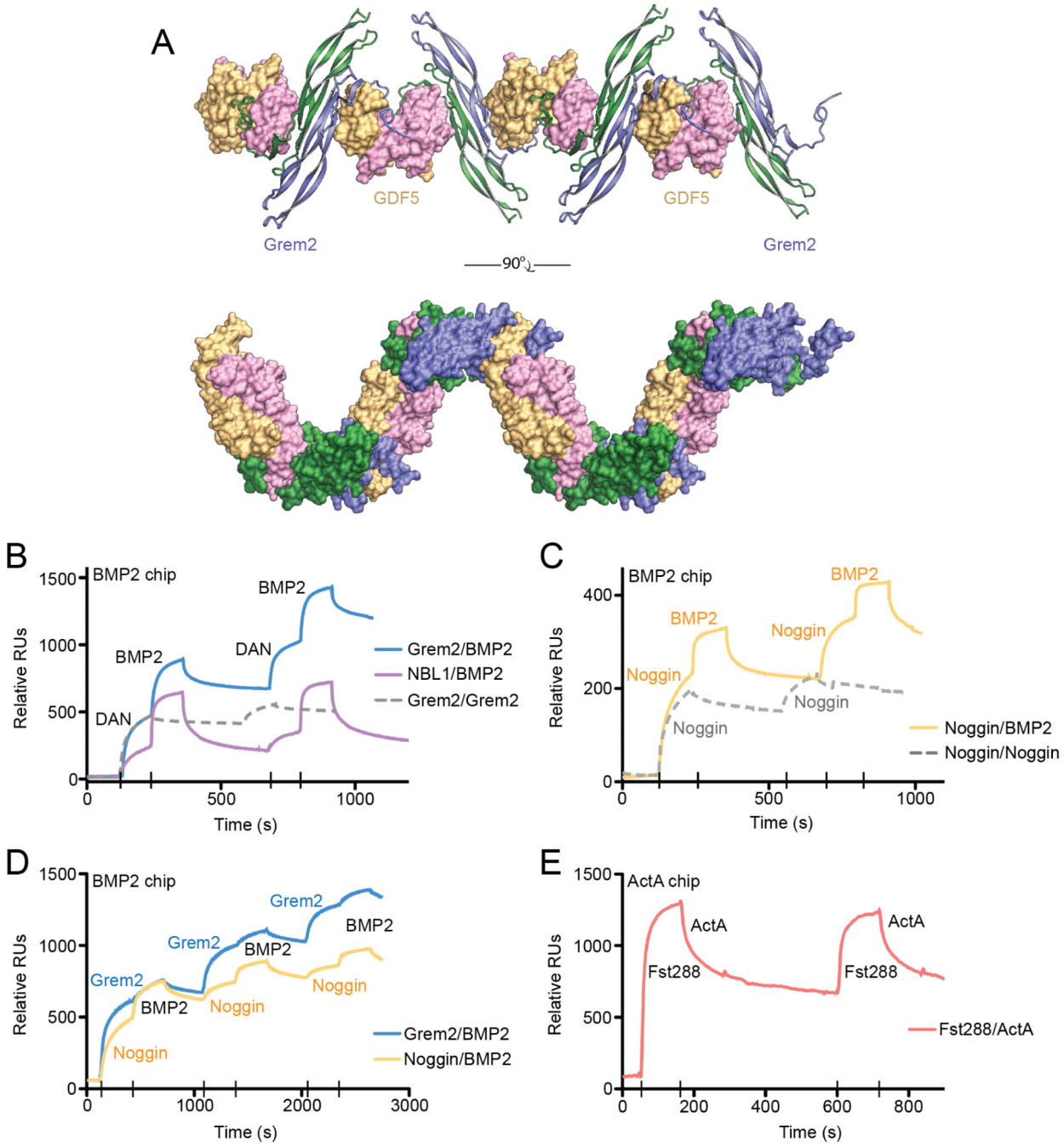

Figure 4. Alternating Aggregation of Grem2-BMP

(A) Grem2-GDF5 complex colored as in Figure 1 forms a continuous alternating complex extending beyond the ASU. (B-D) SPR co-injection studies of antagonist and BMP2 over immobilized BMP2. Antagonists were injected followed by alternating injections of BMP2 and antagonist (all at 500 nM). Control experiments show consecutive injections of antagonist. (B) Analysis of Grem2 and NBL1 and (C) Noggin. (D) Direct comparison of Grem2 and Noggin at a slower flow rate with a longer association time. (E) Similar SPR

experiment with immobilized Activin A and alternating injections of Follistatin and Activin A. Tic marks and labels show specific protein and time of injection.